IEEE Access
Multidisciplinary | Rapid Review | Open Access Journal

Received January 18, 2020, accepted January 28, 2020, date of publication February 5, 2020, date of current version February 17, 2020.

Digital Object Identifier 10.1109/ACCESS.2020.2971685

Synchronous Reluctance Motors With an Axially Laminated Anisotropic Rotor as an Alternative in High-Speed Applications

VALERII ABRAMENKO, ILYA PETROV, JANNE NERG, (Senior Member, IEEE), AND JUHA PYRHÖNEN, (Senior Member, IEEE)

Electrical Engineering Department, Lappeenranta University of Technology, 53850 Lappeenranta, Finland

Corresponding author: Valerii Abramenko (valerii.abramenko@lut.fi)

This work was supported by the Lappeenranta University of Technology.

ABSTRACT The performance capabilities of an axially laminated anisotropic rotor (ALA) in a high-speed synchronous reluctance motor (SynRM) were studied. A 12 kW ALASynRM was designed as an alternative to a high-speed induction motor (IM) with a solid rotor. The electromagnetic design was implemented taking into account possible issues related to the new manufacturing methods, which require thicker rotor layers than in a typical ALA. The ALASynRM shows a higher efficiency than the corresponding IM with a smooth or slitted solid rotor equipped with copper end rings. To verify the design method, a prototype IM with a smooth solid rotor was built and tested. In the analysis, it was found that, similar to IMs, in an ALASynRM a considerable part of losses takes place in the rotor despite the absence of slip-related losses in the SynRM. The distribution of eddy current losses in the ALA rotor is significantly uneven. The torque ripple in the ALASynRM is considerably larger than the corresponding ripple in IMs.

INDEX TERMS 2D simulation, axially laminated anisotropic rotor, ALASynRM, eddy current, high speed, high efficiency, inductance difference, saliency ratio, solid rotor induction motor, slits, slot harmonics, synchronous reluctance motor.

I. INTRODUCTION

As a result of technological development in different fields, high-speed electrical machines have become an attractive solution for many applications. Present electromagnetic design approaches, availability of robust materials (with satisfactory electromagnetic properties), and advancements in power electronics have made high-speed machines more favorable for many applications [1]. High-speed electrical machines are required in installations where a high rotational speed or a high power density are of importance. These motors are used in various applications, such as gas compressors [2], [3], air compressors and blowers [4], microturbines [5], flywheel energy storage systems [6], high-speed spindles [7], and aircraft [8]. In high-speed applications, different types of electrical machines are used, each type having its advantages, disadvantages, and limitations.

An induction motor (IM) with a solid rotor is, in principle, a robust and reliable machine type. These features make an IM one of the main options in high-speed applications. In order to obtain the highest possible efficiency and an acceptable torque-producing capability of a solid rotor not equipped with a copper cage, the rotor should be made of a ferromagnetic material that has a high permeability, a high saturation flux density level, and a low resistivity. Typically, the resistivity of ferromagnetic materials is much higher than the resistivity of nonmagnetic metals such as aluminum or copper [1], [9]. Therefore, the rotor can be additionally equipped with a highly conductive nonmagnetic metal squirrel cage (or only end rings to minimize the end effect) to increase the torque-producing capability and efficiency. Consequently, the rotor will be more complicated, and either its mechanical robustness will decreases, or more expensive materials and much more challenging manufacturing methods must be used [10]. In an IM equipped with a squirrel cage, the rotor maximum surface speed is 200 m/s, which is half of that of the IM with a solid rotor, where the rotor maximum surface speed is 400 m/s [11]. Manufacturing a squirrel-cage high-speed rotor may be very demanding and expensive, especially with large rotor sizes. The main problems related to the squirrel cage are

The associate editor coordinating the review of this manuscript and approving it for publication was Pinjia Zhang.

the low tensile strength of copper or aluminum and different thermal expansion coefficients compared with the solid core material. These factors pose challenges in the design and manufacture of a squirrel-cage solid rotor.

Another conventional method to enhance the performance of a solid-rotor IM is to use axial slits in the rotor, which clearly improve the rotor performance compared with a smooth solid rotor, yet degrade the rigidity of the rotor.

Coating the solid IM rotor with a special material can improve the rotor robustness, allowing operation at a rotor surface speed up to 550 m/s [11]. In addition, coating reduces the impact of the air-gap flux density harmonics. However, it complicates the manufacturing process, and the slip-related rotor losses still limit the motor performance [12].

These facts restrict the use of IMs in applications where high performance characteristics, moderate cost, and robustness are required. Alternative motor layouts may thus be of interest.

Much research has focused on high-speed permanent magnet synchronous machines (PMSM) [13]–[15]. The PM motor can provide superior power density and electrical efficiency. However, increasing the efficiency by permanent magnets involves significant manufacturing and material costs [16]. Furthermore, the robustness of the rotor with permanent magnets is limited.

In the case of embedded magnets in a laminated rotor core, the maximum rotational speed is limited as the integrity of the rotor is determined by the magnet-retaining ribs, which must be thick enough to provide mechanical robustness. On the other hand, the ribs should be as thin as possible to minimize the magnetic short-circuiting of the magnets. If surface magnets are used, strong mechanical integrity is achieved by using sleeves made of materials with a high mechanical strength, such as Inconel, titanium, or carbon fiber, which complicate the rotor structure [1], and, in the case of carbon fiber band, deteriorate the rotor cooling.

Another drawback of permanent magnets is their sensitivity to high temperatures, at which the magnetic properties deteriorate. There are magnets with high temperature tolerance that are capable of operating at 350°C or even up to 550°C. However, magnets capable of operating at higher temperatures typically have a lower remanence and a higher cost compared with other magnets more vulnerable to temperature [1]. Therefore, in the design of a high-speed PMSM, when aiming at a trade-off between electromagnetic performance and cost, some other electrical machine topologies may come into question.

Switched reluctance machines (SRM) can be considered an option in high-speed applications operated in harsh environments, for example, in gas turbines of aircraft [17]. However, a low efficiency and high torque ripple compared with the IM and the PMSM make the SRM not a preferred choice unless there is a specific reason, such as high ambient temperature [18].

Because of the electromagnetic performance limitations in IMs and SRMs, the economic disadvantages of PMSMs, and manufacturing and mechanical limitations of all these machine types, other alternatives such as axially laminated anisotropic rotor synchronous reluctance motors (ALASynRM) have to be considered. Manufacturing of an ALA rotor for a SynRM may be easier and cheaper than manufacturing of a solid rotor equipped with a squirrel cage. In this paper, the suitability of the ALASynRM for further research is investigated.

The rotor of an ALASynRM consists of a stack of magnetic and nonmagnetic layers, which makes it highly anisotropic. The concept of such a rotor is presented in Fig. 1. The high inductance difference and saliency allow minimization of the Joule losses in the stator winding.

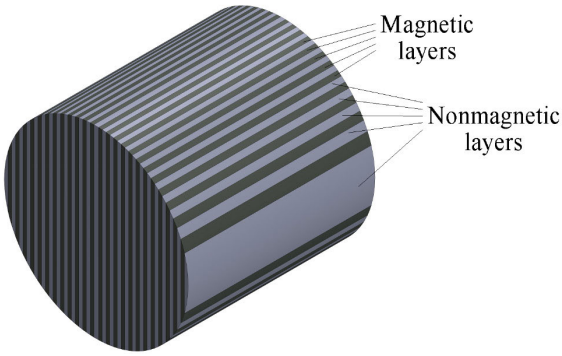

FIGURE 1. Axially laminated rotor of a high-speed SynRM.

The topic of ALASynRMs has been extensively studied [19]–[24]. The main findings are that the ALASynRM is capable of providing a higher efficiency than the IM of a similar frame size. The main benefit is the very small losses in the rotor part. There are no slip-related losses in the rotor of a SynRM, and also the eddy current losses in the rotor are quite low when the rotor is made of thin laminated sheets. This has a positive effect on both the efficiency and the thermal condition of the motor. Some other aspects, such as the impact of the ratio of magnetic material to nonmagnetic material, have been studied [21]–[23]. Another significant benefit of the ALASynRM is the capability to achieve very high saliency ratios, which allows achieving a high power factor and minimization of the winding Joule losses. Some studies have shown that saliency values higher than 20 can be achieved [20], [25].

In the papers on ALASynRMs, the rotor is made of relatively thin magnetic and nonmagnetic layers. The thin layers provide several benefits: a high saliency, minimization of rotor eddy current losses, and low torque ripple. However, the layers are held together by austenitic bolts, which essentially limits the maximum rotational speed of the rotor because of the mechanical strength limit of the screws.

The objective of the current research is to theoretically evaluate the electromagnetic performance of a solid-rotor ALASynRM as a motor for high-speed applications. To ensure a solid construction, metallic bonds between the nonmagnetic and ferromagnetic layers are needed. Thus,

specific rotor manufacturing methods are required. They include hot isostatic pressing, explosion welding, and vacuum brazing. These methods potentially provide a stronger robustness compared with methods where the rotor layers are fixed with bolts and ultimately, at least in principle, the laminated construction should be as strong as a solid material. In our case, a 2-pole 12 kW ALASynRM is studied. As a reference for the ALASynRM design, a 12 kW IM with a solid rotor with copper end rings is used. The main results of the present ALASynRM research are: the ALASynRM provides a higher efficiency than the IM with a smooth solid rotor and the IM with rotor slits, and the efficiency of the high-speed ALASynRM is mainly determined by the rotor eddy currents and the stator iron losses.

The content of the paper is the following. In section II, the selection of the calculation approach and the materials of the ALA rotor are described. Section III provides a performance comparison of the IMs with smooth and slitted solid rotors with the ALASynRM (which has a similar stator as the IMs). The conclusions are drawn in section IV, where the main achievements of the study are discussed.

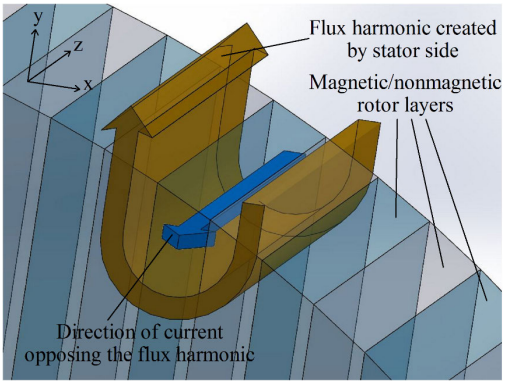

FIGURE 2. Rotor currents induced by flux harmonics.

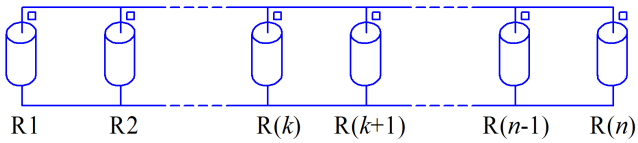

FIGURE 3. Electrical circuit of the rotor. The solid conductors R1…R(n) correspond to the rotor magnetic and nonmagnetic layers.

II. MAIN ASSUMPTIONS AND LIMITATIONS IN CALCULATION

The validity of the calculation method and its possible impacts on the results are discussed in this section. Furthermore, the properties of materials suitable for the rotor of a high-speed ALASynRM are considered taking into account manufacturing aspect. Based on the electromagnetic, thermal, and mechanical properties, suitable materials are selected.

A. CALCULATION APPROACH

As both the magnetic and nonmagnetic layers constituting the rotor are made of steel (having fairly high electrical conductivity, from about 0.5 to 4 MS/m), the rotor is prone to rotor-surface eddy current losses. The currents induced in the rotor have a path to flow along the layers and between the layers depending on the direction of the induced voltage. In principle, such a rotor structure requires 3D analysis. However, because of the high simulation time and processing power demand of the 3D analysis, 2D simulation was applied in this study; the validation of the 2D approach adopted in this study is given in the following.

The flux harmonics mainly travel along a 2D plane (referred to as the xy -plane), and the induced currents tend to flow along the normal of that plane (referred to as the z-direction). This principle is illustrated in Fig. 2. The only place where the non-z-directed currents may reach significant values is the rotor core close to the edge of the stator core. In order to compensate for neglecting the rotor currents along the x- and y-directions in the 2D model and to allow a free flow of currents between the layers, all the layers assigned to solid conducting regions were short-circuited at the ends in the model (Fig. 3). However, in reality, the impedance between two random layers is determined by the distance between the layers, the frequency of eddy currents, the permeability of steel, and other factors, which cannot be taken into account in the 2D simulation. If the eddy current harmonics are mainly caused by the stator slotting effect as the winding harmonics are minimized by short pitching, the eddy current path at the rotor edge is relatively short (equals the slot pitch), which allows to neglect the factors impacting the eddy current impedance yet without a significant loss in calculation accuracy.

The IMs were also simulated in 2D, where the solid rotor was assigned to a solid conducting region. The path for eddy current losses at the rotor edge was treated similarly as in the ALASynRM, meaning that the rotor edge impedance was neglected. In the study, IMs with copper end rings attached to the rotor ends were considered. As the copper resistivity is less than one-tenth of the resistivity of S355 (rotor core material), the assumption of short-circuited ends of the rotor should not significantly affect the results. After all, with a larger real rotor impedance (where the non-z-directed currents occur), the IM should operate with a larger slip, yielding higher slip-related losses. This means that the overall losses of the IM may be somewhat too optimistic in the calculations, which should be kept in mind when comparing the ALASynRM and the IM in terms of efficiency.

In the Flux2D software package, the eddy current losses in the rotor are estimated similarly as Joule losses in any conducting material by the following equation

$$P_{\text{Joule\_cond}} = \int_V \frac{J^2}{\sigma} \mathrm{d}V, \tag{1}$$

where J is the current density in the material, σ is the conductivity of the material, and V is the volume of the material.

The iron losses in the stator stack are calculated by the Bertotti loss separation model for the power density in iron

using a stacking factor of an iron core that takes into account the electrical insulation in the lamination

$$dP_{iron} = \left(k_h B_m^2 f + \frac{\pi^2 \sigma d^2}{6} (B_m f)^2 + k_e (B_m f)^{\frac{3}{2}} \cdot 8.67\right) \cdot k_f, \quad (2)$$

where k_h is the coefficient of hysteresis losses, k_e is the coefficient of excess losses, σ is the conductivity of the material, d is the thickness of the lamination, f is the frequency, B_m is the peak value of the magnetic flux density, and k_f is the lamination space factor.

B. SELECTION OF THE ROTOR MATERIALS

The material of the rotor magnetic and nonmagnetic layers should be selected considering not only the electromagnetic and mechanical properties but also the manufacturing technology. The rotor can be manufactured by means of hot isostatic pressing, explosion welding, or vacuum brazing. When applying these technologies, the thermal expansion factors of the magnetic and nonmagnetic layers should be as close to each other as possible. Otherwise, when cooling the rotor after compounding the layers, the residual stresses can spoil the rotor construction. In this study, a combination of S355 and Inconel 718 was selected. The magnetic steel material S355 was selected as its suitability as a solid rotor core material in IMs has been shown in practice [9], [12]. The nonmagnetic material Inconel 718 was chosen based on its compatibility with S355 (similar thermal expansion coefficient). The main data of the rotor materials are provided in Table 1. The measured *BH*-curve of S355 (equivalent to the previous standard Fe52) is provided in [9]. An obvious problem related to this material pair is that the tensile strength of S355 is significantly lower than that of Inconel 718.

TABLE 1. Properties of S355 and Inconel 718.

Symbol	S355	Inconel 718
Initial relative permeability	≈1000	1.001 (max)
Saturation flux density, (T)	1.9	–
Electrical resistivity, (Ohm·m)	$25.7 \cdot 10^{-8}$	$124.9 \cdot 10^{-8}$
Temperature coefficient of resistivity, (1/K)	0.0038	0.00024
Thermal expansion coefficient, (1/K)	$12.5 \cdot 10^{-6}$	$12.8 \cdot 10^{-6}$
Tensile yield strength, (MPa)	300	1100
Tensile ultimate strength, (MPa)	520	1375
Mass density, (kg/m^3)	7870	8190

III. DESIGN OF THE ALASynRM AS AN ALTERNATIVE TO THE IM WITH A SOLID ROTOR AND THE IM WITH A SLITTED ROTOR

A. INITIAL DATA OF THE MOTORS UNDER STUDY

The main boundary condition that was preselected in the design of the high-speed ALASynRM is the number of poles. The manufacturing methods suitable for the high-speed ALASynRM are easier to apply to a two-pole rotor, as there are fewer degrees of freedom in comparison with the rotors where the number of poles is larger. This means that a two-pole rotor is less likely to deform during manufacturing. Moreover, a two-pole SynRM has a larger inductance difference than machines where the number of poles is larger [23], [26]–[27]. In addition, a 2-pole machine needs less electrical frequency (e.g. compared with 4-pole machines), which allows to eliminate limitations set by a frequency converter (which has a limited output frequency).

There are several ways to carry out the shaft mounting. The first option is to make the rotor billet long enough to mill the shaft from the same material as the rotor. The second alternative is to attach austenitic ends to the active core by friction welding. The benefit of an austenitic shaft is that the layers will not be magnetically shortened at the active part ends. The third method to attach the shaft ends is welding, for instance electron beam welding. The fourth option is to attach austenitic shaft ends during the initial manufacturing of the rotor billet.

In this case, a 12 kW ALASynRM was studied as a proof-of-concept machine. As a reference, a 12 kW IM with a smooth solid rotor with copper end rings was used. The data of the IM are given in Table 2. It was assumed that mechanical robustness is achieved, the rotor operating temperature is 100°C, and the electrical properties (conductivity) of the materials correspond to the thermal condition in question. The stator of the designed ALASynRM was the same as in the IM, and only the rotor was replaced by an ALA rotor. The air-gap length was kept 1 mm for all the machines, and thus, also the rotor diameter was the same.

TABLE 2. Parameters of the 12 kW Induction motor with a solid rotor.

Motor parameter	Value
Number of pole pairs	1
Number of phases, m	3
Number of stator slots, Q_s	24
Number of winding layers	2
Number of turns in series	24
Number of parallel branches, a	2
Winding factor, k_{w1}	0.925
Short-pitching ratio, W/τ_p	5/6
Stator outer diameter, (mm)	235
Stator inner diameter (bore), (mm)	100.5
The slot opening width, (mm)	1.4
Stator length, (mm)	100
Stator effective length, (mm)	96
Ventilation duct width, (mm)	4
Air-gap length, δ (mm)	1
Rotor diameter, D_r (mm)	98.5
Rotor length, mm	100
Nominal line-to-line voltage, U_s (V)	225
Connection	delta
Nominal current, I_s (A)	37.5/65
Peak current density in the slot, J, (A/mm^2)	2.42
Nominal frequency, f (Hz)	400
Stator AC resistance, R_s (mOhm) 20 °C, 400 Hz	39
Stator leakage inductance, $L_{s\sigma}$ (μH)	121
Rotor material: S355.	
Stator material: NO20-13 [29]. The Berotti coefficients used in simulation: $k_h = 265.5$; $k_e = 0.001$; $k_f = 0.98$; $\sigma = 1612903.22$ S/m	

Additionally, for a more comprehensive comparison between the ALASynRM and the IM, an IM with a slitted solid rotor with copper end rings was designed. The procedure of the slitted IM design has been extensively studied, and in the current case, the design was implemented according to the recommendations found in [12]. The width of the slits was chosen to be 2.5 mm, which is close to the practical minimum width from the viewpoint of low-cost manufacturing. To achieve close to the highest electromagnetic performance, the rule of thumb is to have the depth of slits to about 50% of the rotor radius [28], which was also assumed in the current case. However, the mechanical analysis showed that the safety factor is only 1.1 (Fig. 4), which can hardly be practically accepted. Therefore, the obtained electromagnetic performance of the slitted IM is certainly overestimated. The best results were obtained with 28 slits.

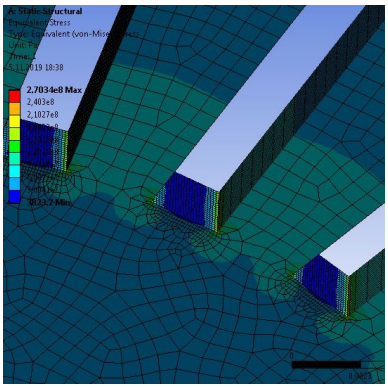

FIGURE 4. Mechanical analysis of an IM rotor with 28 slits. The peak of the von Mises stress is 270 MPa.

The study of the ALASynRM was carried out with 2 mm thick layers. When considering a manufacturing technology involving heat treatment such as hot isostatic pressing, explosion welding, and vacuum brazing, layers that are thinner than 2 mm may not be feasible from the manufacturing viewpoint. To maximize the saliency of the motor, the outermost q-axis layers have to be nonmagnetic to minimize the q-axis inductance. The maximum d-axis current linkage acts along the physical d-axis of the rotor, and thus, it is advisable to have a magnetically conducting layer along the physical d-axis. The sum of the 2 mm layers does not equal the 98.5 mm diameter; if the assembly of the motor is started from the outermost layers (which are nonmagnetic), it turns out that the middle layer has to be 2.5 mm, and it is nonmagnetic. However, according to the chosen rotor arrangement that is based on the current linkage distribution along the d-axis, the middle layer of 2.5 mm is assigned to the magnetic material, yielding a total thickness of 6.5 mm for the magnetic middle layer. It is also closer to a real case because the middle layer, experiencing the largest centrifugal force, should be wider owing to the mechanical constraints. The geometry of the described ALASynRM rotor topology is shown in Fig. 5. The simulation of the ALASynRM was implemented with the maximum torque per ampere (MTPA) control.

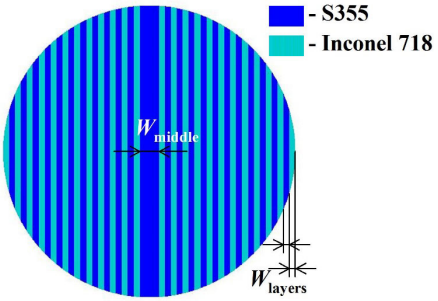

FIGURE 5. Design of the rotor structure. $W_{middle} = 6.5$ mm. $W_{layers} = 2$ mm.

All the rotor geometrical parameters of the machines to be studied are provided in Table 3. The masses of the active materials in the machines are listed in Table 4.

TABLE 3. Rotor geometrical parameters of the motors under study.

Rotor parameter	Smooth solid-rotor IM	Slitted solid-rotor IM	ALASynRM
Rotor radius, (mm)	49.25	49.25	49.25
Slit depth, (mm)	-	24.63	-
Slit width, (mm)	-	2.5	-
Layer thickness, (mm)	-	-	2
Middle layer thickness, (mm)	-	-	6.5

TABLE 4. Masses of active materials in the motors under study.

Motor part	Smooth solid-rotor IM	Slitted solid-rotor IM	ALASynRM
Stator iron, (kg)	23.34	23.34	23.34
Stator copper, (kg)	5	5	5
Rotor, (kg)	6	4.64	6.11
S355 in the rotor, (kg)	6	4.64	3.16
Inconel 718 in the rotor, (kg)	-	-	2.95

B. VALIDATION OF THE SIMULATION RESULTS

An IM prototype with a smooth solid rotor was built and tested. A schematic diagram of the workbench is given in Fig. 6. An inverter supplies a rotating converter (IM/SM) producing sinusoidal output at a variable frequency. A Philips PM 6670 frequency counter measures the voltage frequency. The generator stator winding is connected to a three-phase transformer to adapt the voltage range.

The supply circuit is connected to the test machine, a 12 kW IM with a smooth solid rotor, through Norma D 5155 power analyzer (M1 in Fig. 6). The test motor is loaded with a WB 65-HS eddy-current dynamometer (ECD) with water cooling. The measured motor and dynamometer are connected by a mechanical flexible coupling. A Vibro Meter 234-213-000 eddy-current brake (M3 in Fig. 6) is used to measure torque, speed, and shaft power delivered by the tested machine. Photographs of the disassembled prototype motor are provided in Fig. 7, and Fig. 8 depicts the dynamometer and the mechanical coupling.

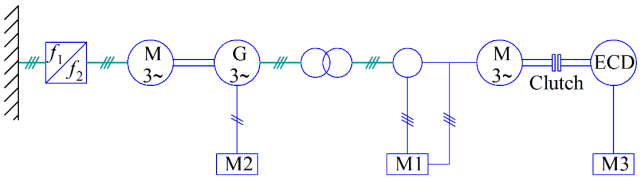

FIGURE 6. Workbench to test the IM with a smooth solid rotor.

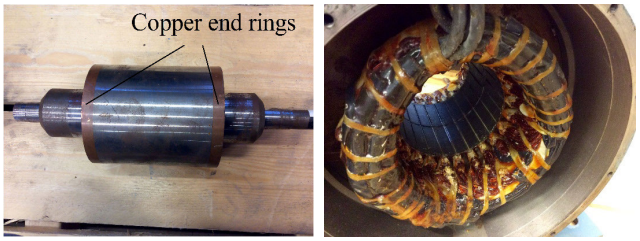

a) Rotor b) Stator

FIGURE 7. Prototype of the 12 kW induction motor.

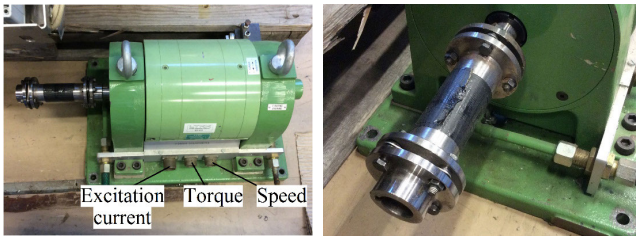

a) Dynamometer b) Coupling

FIGURE 8. Dynamometer and mechanical coupling. The dynamometer has an input for excitation current and outputs for torque and speed data.

A comparison of the no-load losses is given in Table 5. We can see that there is no significant difference in total losses between the simulated and measured results. The larger losses obtained in measurements can be explained by the additional losses caused by windage and friction. The no-load measurements were conducted without a coupling dynamometer.

A loss comparison at a 4 Nm motor torque is provided in Table 6. We can see that the loss difference between the simulated and measured results is 499 W. According to the no-load test, 73 W of the losses is due to the friction and windage losses of the motor itself. The coupling system has four cylindrical disks; such a system is an additional source of windage losses, which amount to a few hundred extra watts. This explains the mismatch between the measured and calculated losses in Table 5; however, it is challenging to define the exact location and value of losses.

The test results show that the FEA of the induction motor is reliable. We may thus believe that also the SynRM can be analyzed similarly as all the parts except the rotor are the same.

C. PERFORMACE ESTIMATION AT THE RATED OPERATING POINT

The results of the simulated 12 kW IMs and ALASynRM are given in Table 7.

TABLE 5. Comparison of the no-load losses of the 12 kW Induction Motor with a solid rotor obtained by simulation and measurements.

Parameter	Simulation	Test
Speed, (rpm)	24000	24000
Stator winding losses, (W)	31.97	-
Stator iron losses, (W)	168.37	-
Rotor Joule losses, (W)	41.99	-
Total losses, (W)	242.33	315
Difference in total losses compared with the test results, (W)	-72.67	0

TABLE 6. Comparison of the losses of the 12 kW Induction Motor with a solid rotor obtained by simulation and measurements.

Parameter	Simulation	Test
Output power*, (kW)	10.01	10
Torque, (Nm)	4.01	4
Stator winding losses, (W)	101.72	-
Stator iron losses, (W)	168.07	-
Rotor Joule losses, (W)	429.57	-
Total losses, (W)	699.36	1198.21
Difference in total losses compared with the test results, (W)	-498.85	0
Efficiency, (%)	93.47*	89.3**

* Coupling windage excluded

** Coupling windage included

The ALASynRM has smaller stator winding Joule losses and a higher power factor than the solid-rotor IMs. It is worth mentioning that the MTPA logic does not provide the largest power factor. The possible maximum power factor of the ALASynRM is 0.859 according to the equation [30]

$$\cos(\varphi)_{\max} = \frac{L_d/L_q - 1}{L_d/L_q + 1}, \tag{3}$$

where L_d is the d-axis inductance, and L_q is the q-axis inductance.

The possibility of operating with such a large power factor is explained by the low q-axis inductance (low q-axis armature reaction) and the high d-axis inductance, which is only 17.9% lower than the magnetizing inductance of the IM, even though the amount of magnetic conducting material in the rotor of the ALASynRM is about half of that in the IM. The high value of the d-axis inductance of the ALASynRM is explained by the low flux density level in the rotor. The low q-axis inductance is ensured by a significant amount of nonmagnetic material placed across the q-axis. In fact, the maximum power factor can be even somewhat higher with the non-MTPA control, where the q-axis current is higher than the d-axis current. In this case, the d-axis inductance should be higher because of the lower saturation of the d-axis path, and the q-axis inductance should be lower because of the stronger saturation of the q-axis path.

TABLE 7. Comparison of the Performances of the 12 kW Induction Motor with a solid rotor and the 12 kW ALASynRM.

Parameter	Smooth solid-rotor IM	Slitted solid-rotor IM	ALASynRM
Output power*, (kW)	12	12	11.8
Speed*, (rpm)	23806.8	23910.97	24000
Torque*, (Nm)	4.81	4.81	4.71
Peak-to-peak torque ripple, (Nm)	0.03	0.278	2.03
Rated phase current RMS, (A)	33.8	29.67	27.89
Magnetizing inductance, (mH)	5.34	4.5	-
d-axis synchronous inductance, (mH/pu)	-	-	4.43/1.38
q-axis synchronous inductance, (mH/pu)	-	-	0.34/0.1
Inductance difference, (mH)	-	-	8.19
Saliency, L_d/L_q	-	-	13.14
Stator winding losses, (W)	133.62	103.03	90.98
Stator iron losses, (W)	168.07	176.99	172.66
Rotor Joule losses, (W)	593.83	226.91	201.72
Total losses, (W)	895.53	506.92	465.36
Efficiency, (%)	93.05	95.96	96.21
Power factor	0.583	0.641	0.674

* values obtained by the FEA with 12 kW output as the target

In Fig. 9, the flux density distributions in the IMs and the ALASynRM are presented. In the rotor of the IM with the smooth solid rotor, the flux is unevenly distributed because the currents induced in the rotor try to displace the flux on the rotor periphery. The flux density in the rotor decreases from 1.8 T on the periphery (neglecting local saturation near the stator slots, where the flux density is above 2 T) to about 0.1 mT in the middle of the rotor.

In the rotor of the IM with the slitted rotor, the reluctance for the flux in the tangential direction is stronger, which forces the flux to penetrate deeper into the rotor. There is a local saturation in the area near the bottom of the slits. However, the flux density, and consequently, the rotor eddy current distribution in the whole rotor area, are more even than in the smooth rotor. As a result, eddy currents in the slitted rotor experience a lower resistance than in the smooth solid rotor. Thus, it is possible to provide the required torque at a lower slip. The IM with the slitted rotor has a higher power factor than the IM with the smooth rotor. Less magnetizing current (and total stator current) is required for operation at a lower slip with the slitted rotor, even though the no-load magnetizing inductance of the smooth-rotor machine is larger than that of the slitted rotor.

In the rotor of the ALASynRM, the flux distribution is nearly uniform because the fundamental harmonic of the air-gap flux density rotates synchronously with the rotor, and no induced currents oppose the fundamental flux in the rotor of the machine. The flux density level in the magnetically conducting segments is about 1.2 T.

Stator iron losses are the largest in the IM with the slitted rotor, which distorts the air-gap flux density. The

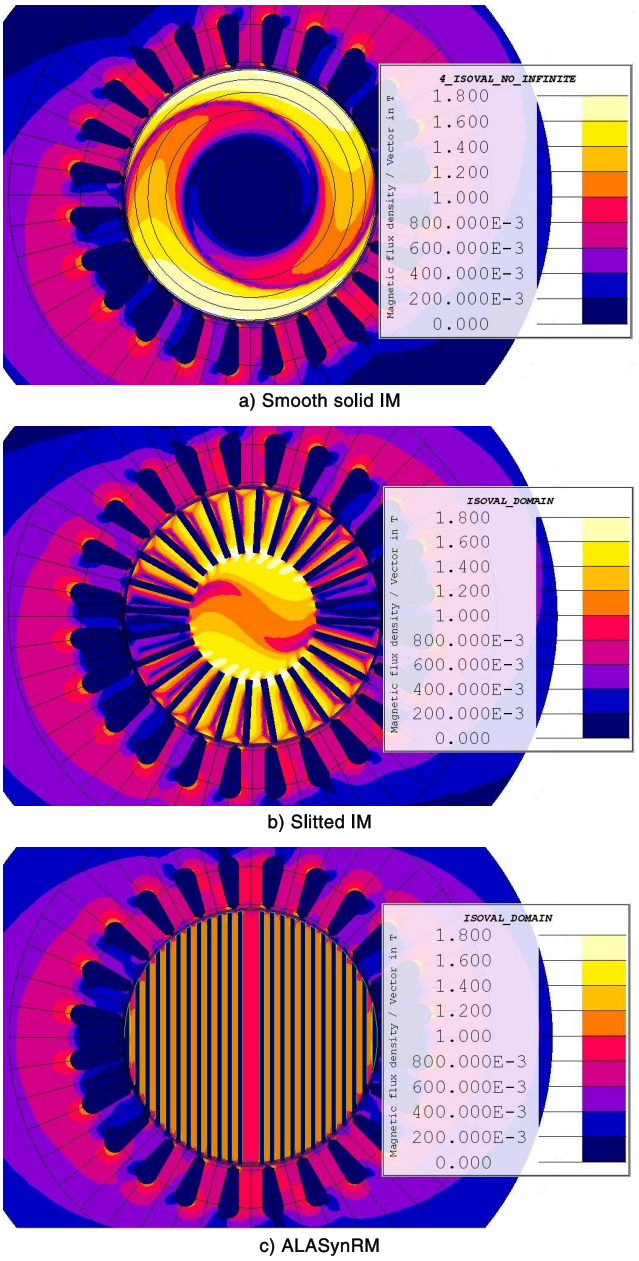

FIGURE 9. Flux density distributions in (a) smooth solid rotor IM, (b) slitted solid rotor IM, and (c) ALASynRM at rated load.

ALASynRM has larger stator iron losses than the IM with the smooth solid rotor, which is predictable because of the permeance harmonics in the air-gap flux density caused by the rotor anisotropic structure. Even though the flux density in the stators of the motors is relatively small and the stator is far from saturation, the iron losses account for a significant proportion of the total losses, which is common in high-speed machines because of the high operating frequency.

Rotor losses in the slitted IM are smaller than in IM with the smooth solid rotor because of the lower rated slip. Further, the slitted rotor structure is highly reluctant for spatial harmonics, thus minimizing the rotor eddy current losses

caused by the slot effect. The rotor losses in the ALASynRM are eddy current losses caused by the stator winding and permeance harmonics. Because of the synchronous rotation, there are no slip-related losses, and the total rotor losses are significantly smaller than in the IMs. The current density distribution, which determines the rotor eddy current losses, is given for the IMs and the ALASynRM in Fig. 10. The current density distribution is in agreement with the flux density distribution in Fig. 6. We can see that in the IM with the smooth solid rotor, the rotor eddy current losses are determined by the fundamental flux density (slip-related losses) and the stator slot harmonics, which is evidenced by the current density concentrations on the rotor periphery with the stator slot periodicity. In the case of the slitted IM, not only the slip-related losses are reduced, but also the losses caused by the slot harmonics are minimized, because the number of slits is larger than the number of slots, and the main part of the stator slot flux density harmonics is efficiently blocked by the rotor slits. In the ALASynRM, there are no slip-related losses as the rotor rotates synchronously, but substantial eddy current losses are produced by the stator slot flux density harmonics, which can be seen from the current density distribution, where the direction of current varies with the stator slot periodicity.

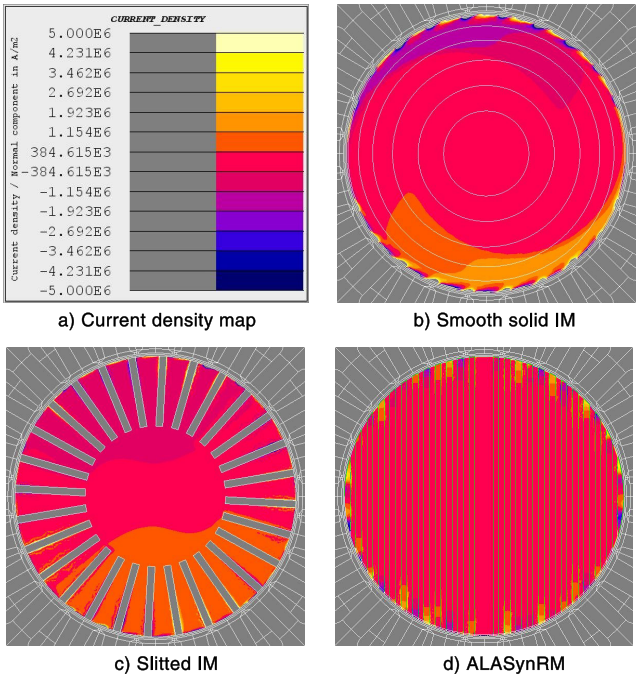

FIGURE 10. Current density distributions in (b) smooth solid rotor IM, (c) slitted solid rotor IM, and (d) ALASynRM at rated load.

The loss distribution in each layer is given in Fig. 11. The losses increase in the direction from the middle layer towards the sides, because a larger layer area experiences the flux density harmonics. The peak of the losses in the middle layer is explained by its higher thickness (6.5 mm instead of 2 mm). It is noteworthy that the losses in the Inconel 718 layers are

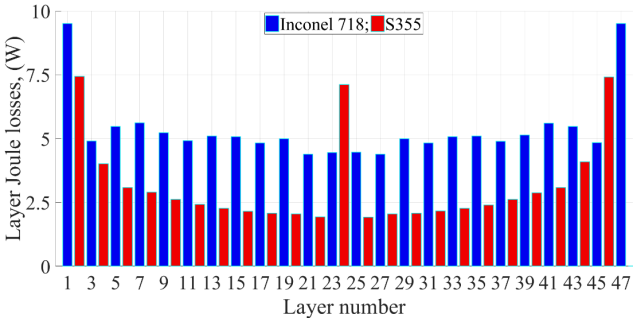

FIGURE 11. Loss distribution in the rotor layers.

larger than in S355. The resistivity of Inconel 718 is about five times as high as the resistivity of S355, and therefore, the skin effect in S355 is more manifested. Thus, the smaller losses in S355 can be explained by the fact that the low-resistive S355 displaces eddy currents more strongly on the surface, which results in a larger resistance of the circuit where the eddy current circulate. However, a detailed analysis of the eddy current losses in the rotor of the ALASynRM is not in the scope of this paper.

The comparison of torque ripple in the motors was based on the peak-to-peak torque ripple. In the IM with the smooth solid rotor, the torque ripple is negligibly small (less than 0.1%), and in the slitted IM it is 5.8%, as the interaction of the rotor slits with the stator teeth produces a cogging torque component. The torque ripple is much stronger in the ALASynRM than in the IMs. In the ALASynRM, the torque ripple reaches even 43.1% of the rated torque. The motor torque calculated as a function of rotational angle is given in Fig. 12. The strong torque pulsations are due to the cogging torque, which occurs as a result of the interaction between the rotor magnetic layers and the slotted stator. The spectrum analysis of the torque is given in Fig. 13. The strongest high-order harmonics are the 24^{th} and 48^{th}, which are proportional to the number of stator slots/teeth. At any instant, the magnetic circuit seeks the relative position between the stator teeth and the rotor magnetic layers where the magnetic energy of the system is minimized. In the case of an IM with a squirrel cage, a same number of rotor and stator slots is strongly not recommended [11]. If the numbers of rotor and stator slots are the same, there are two evident positions where the magnetic system has the maximum or minimum energy of the magnetic circuit, which results in a high torque ripple. The same principle is applicable to IMs with slits [12]. The ALASynRM does not have rotor slots that are radially oriented, but instead, magnetic and nonmagnetic layers that are oriented in the same direction and are not evenly distributed over the rotor periphery. Therefore, each magnetic layer attracts the stator teeth differently. Torque ripple can thus be minimized by adjusting the thickness of the layers, which requires further research. However, in high-speed machines, the negative effects of torque ripple such as jerking or speed ripple are efficiently filtered out by inertia.

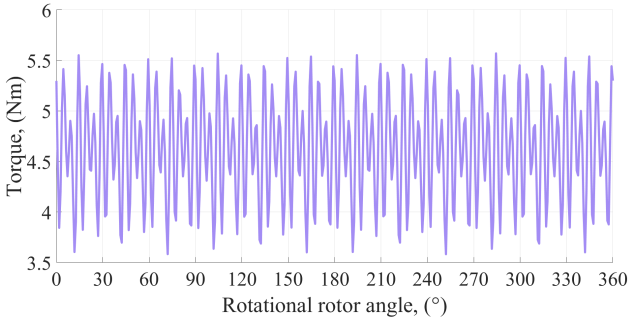

FIGURE 12. Torque as a function of rotational angle at the rated speed of the ALASynRM under study.

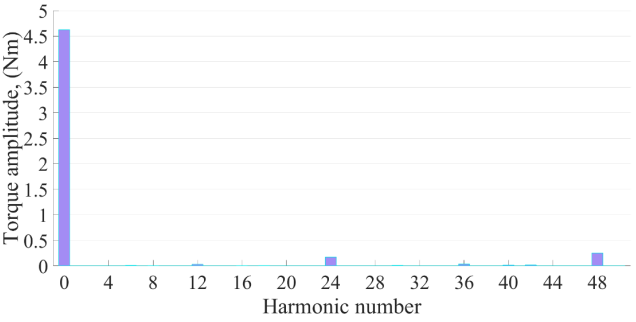

FIGURE 13. Harmonic spectrum analysis of the torque in the ALASynRM under study.

IV. CONCLUSION

As an alternative to a solid-rotor IM, a 12 kW high-speed synchronous reluctance motor with an axially laminated anisotropic rotor was studied. The materials used for the magnetic and nonmagnetic rotor layers were S355 and Inconel 718, respectively, which are assumed to be suitable for temperature-treating manufacturing methods (hot isostatic pressing, explosion welding, and vacuum brazing), as these materials have similar thermal expansion coefficients. When the solid rotor of an IM was directly substituted by an ALA rotor while keeping the stator and air-gap length the same, the ALASynRM showed a 3.16%-unit higher efficiency than the IM with the smooth solid rotor and a 0.25%-unit higher efficiency than the IM with the slitted rotor where both the IM rotors were equipped with copper end rings.

The peak-to-peak torque ripple in the ALASynRM, being 43.1% of the rated torque, was much higher than in the IMs, where it was 5.8% in the IM with slits and less than 0.1% in the IM with the smooth solid rotor. The methods to minimize torque ripple in the ALASynRM, however, call for further study.

In the further research into ALASynRMs, the impact of the rotor geometry on the performance should be considered. Considering the proposed manufacturing methods, a small number of rotor layers is desired. At the same time, the largest loss component is the rotor eddy current loss, which raises the question of the relationship between the number of rotor layers and rotor losses. The distribution of losses in the layers of materials with different resistivities should be considered in more detail. Further, methods to minimize torque ripple in the ALASynRM should be studied. A prototype rotor is required to test the applicability of the technology in a solid-rotor high-speed machine.

REFERENCES

[1] D. Gerada, A. Mebarki, N. L. Brown, and C. Gerada, "High-speed electrical machines: Technologies, trends, and developments," *IEEE Trans. Ind. Electron.*, vol. 61, no. 6, pp. 2946–2959, Jun. 2014.

[2] J. Pyrhonen, J. Nerg, P. Kurronen, and U. Lauber, "High-speed high-output solid-rotor induction-motor technology for gas compression," *IEEE Trans. Ind. Electron.*, vol. 57, no. 1, pp. 272–280, Jan. 2010.

[3] R. Lateb, J. Enon, and L. Durantay, "High speed, high power electrical induction motor technologies for integrated compressors," in *Proc. Int. Conf. Electr. Mach. Syst.*, Nov. 2009, pp. 1–5.

[4] K. Y. Bell and S. Abel, "Optimization of WWTP aeration process upgrades for energy efficiency," *Water Pract. Technol.*, vol. 6, no. 2, pp. 1–10, 2011.

[5] L. Goldstein, B. Hedman, D. Knowles, S. I. Freedman, R. Woods, and T. Schweizer, "Gas-fired distributed energy resource technology characterizations," Nat. Renew. Energy Lab., Golden, CO, USA, Tech. Rep. NREL/TP-620-34783, Nov. 2003.

[6] P. I. Tsao, "An integrated flywheel energy storage system with homopolar inductor motor/generator and high-frequency drive," *IEEE Trans. Ind. Appl.*, vol. 39, no. 6, pp. 1710–1725, Nov./Dec. 2003.

[7] C. Zwyssig, J. Kolar, and S. Round, "Megaspeed drive systems: Pushing beyond 1 million r/min," *IEEE/ASME Trans. Mechatronics*, vol. 14, no. 5, pp. 564–574, Oct. 2009.

[8] F. Ismagilov, V. Vavilov, D. Gusakov, and N. Uzhegov, "Topology selection of the high-speed high-voltage PMSM for aerospace application," in *Proc. 43rd Annu. Conf. IEEE Ind. Electron. Soc. (IECON)*, Oct. 2017.

[9] J. Pyrhönen, "The high-speed induction motor: Calculating the effects of solid-rotor material on machine characteristics," Doctoral dissertation, Lappeenranta Univ. Technol., Lappeenranta, Finland, 1990.

[10] J. Barta, N. Uzhegov, P. Losak, C. Ondrusek, M. Mach, and J. Pyrhönen, "Squirrel-cage rotor design and manufacturing for high-speed applications," *IEEE Trans. Ind. Electron.*, vol. 66, no. 9, pp. 6768–6778, Sep. 2019.

[11] J. Pyrhönen, T. Jokinen, and V. Hrabovcova, *Design of Rotating Electrical Machines*, 2nd ed. Chichester, U.K.: Wiley, 2013.

[12] T. Aho, "Electromagnetic design of a solid steel rotor motor for demanding operation environments," Doctoral dissertation, Lappeenranta Univ. Technol., Lappeenranta, Finland, 2007.

[13] N. Uzhegov, E. Kurvinen, J. Nerg, J. Pyrhonen, J. T. Sopanen, and S. Shirinskii, "Multidisciplinary design process of a 6-slot 2-pole high-speed permanent-magnet synchronous machine," *IEEE Trans. Ind. Electron.*, vol. 63, no. 2, pp. 784–795, Feb. 2016.

[14] L. Dang, N. Bernard, N. Bracikowski, and G. Berthiau, "Design optimization with flux weakening of high-speed PMSM for electrical vehicle considering the driving cycle," *IEEE Trans. Ind. Electron.*, vol. 64, no. 12, pp. 9834–9843, Dec. 2017.

[15] M.-S. Lim, S.-H. Chai, J.-S. Yang, and J.-P. Hong, "Design and verification of 150-krpm PMSM based on experiment results of prototype," *IEEE Trans. Ind. Electron.*, vol. 62, no. 12, pp. 7827–7836, Dec. 2015.

[16] A. T. D. Almeida, F. J. T. E. Ferreira, and G. Baoming, "Beyond induction motors—technology trends to move up efficiency," *IEEE Trans. Ind. Appl.*, vol. 50, no. 3, pp. 2103–2114, May/Jun. 2014.

[17] R. Hall, A. Jack, B. Mecrow, and A. Mitcham, "Design and initial testing of an outer rotating segmented rotor switched reluctance machine for an aero-engine shaft-line-embedded starter/generator," in *Proc. IEEE Int. Conf. Electr. Mach. Drives*, May 2005, pp. 1870–1877.

[18] A. Tenconi, S. Vaschetto, and A. Vigliani, "Electrical machines for high-speed applications: Design considerations and tradeoffs," *IEEE Trans. Ind. Electron.*, vol. 61, no. 6, pp. 3022–3029, Jun. 2014.

[19] A. Cruickshank, A. Anderson, and R. Menzies, "Theory and performance of reluctance motors with axially laminated anisotropic rotors," *Proc. Inst. Electr. Eng.*, vol. 118, no. 7, p. 887, 1971.

[20] D. Platt, "Reluctance motor with strong rotor anisotropy," *IEEE Trans. Ind. Appl.*, vol. 28, no. 3, pp. 652–658, May/Jun. 1992.

[21] D. Staton, T. Miller, and S. Wood, "Maximising the saliency ratio of the synchronous reluctance motor," *IEE Proc. B Electr. Power Appl.*, vol. 140, no. 4, p. 249, 1993.

[22] T. Matsuo and T. Lipo, "Rotor design optimization of synchronous reluctance machine," *IEEE Trans. Energy Convers.*, vol. 9, no. 2, pp. 359–365, Jun. 1994.
[23] B. Chalmers and L. Musaba, "Design and field-weakening performance of a synchronous reluctance motor with axially laminated rotor," *IEEE Trans. Ind. Appl.*, vol. 34, no. 5, pp. 1035–1041, Sep./Oct. 1998.
[24] C. Gu, L. Li, K. Shao, and Y. Xiang, "Anisotropic finite element computation of high density axially-laminated rotor reluctance machine," *IEEE Trans. Magn.*, vol. 30, no. 5, pp. 3679–3682, Sep. 1994.
[25] I. Boldea, Z. Fu, and S. Nasar, "Performance evaluation of axially-laminated anisotropic (ALA) rotor reluctance synchronous motors," *IEEE Trans. Ind. Appl.*, vol. 30, no. 4, pp. 977–985, Jul./Aug. 1994.
[26] N. Bianchi and B. Chalmers, "Axially laminated reluctance motor: Analytical and finite-element methods for magnetic analysis," *IEEE Trans. Magn.*, vol. 38, no. 1, pp. 239–245, Jan. 2002.
[27] R. R. Moghaddam, "Synchronous Reluctance Machine (SynRM) in Variable Speed Drives (VSD) Applications," Ph.D. dissertation, KTH Roy. Inst. Technol., Stockholm, Sweden, 2011.
[28] J. Huppunen, "High-speed solid-rotor induction machine electromagnetic calculation and design," Doctoral dissertation, Lappeenranta Univ. Technol., Lappeenranta, Finland, 2004.
[29] Thyssenkrupp. (Feb. 2017). *Steel. General product range*. Accessed: Nov. 10, 2019. [Online]. Available: https://www.thyssenkrupp-steel.com/media/content_1/publikationen/thyssenkrupp_general_product_range_steel_2015_1.pdf
[30] J. Pyrhonen, V. Hrabovcova, and R. S. Semken, *Electrical Machine Drives Control: An Introduction*. Chichester, U.K.: Wiley, 2016.

VALERII ABRAMENKO received the Specialist degree in electrical drives and automation of industrial installations from South Ural State University (SUSU), Chelyabinsk, Russia, in 2014, and the M.Sc. degree in electrical engineering jointly from SUSU and the Lappeenranta University of Technology (LUT), Lappeenranta, Finland, in 2017.

He is currently a Researcher with the Department of Electrical Engineering, LUT. His research interest includes high-efficient synchronous motors.

ILYA PETROV received the D.Sc. degree from the Lappeenranta University of Technology (LUT), Finland, in 2015. He is currently a Fellow Researcher with the Department of Electrical Engineering, LUT.

JANNE NERG (Senior Member, IEEE) received the M.Sc. degree in electrical engineering, the Licentiate of Science (Technology) degree, and the D.Sc. (Technology) degree from the Lappeenranta University of Technology (LUT), Lappeenranta, Finland, in 1996, 1998, and 2000, respectively.

He is currently an Associate Professor with the Department of Electrical Engineering, LUT. His research interests are in the field of electrical machines and drives, especially electromagnetic, and thermal modeling and design of electromagnetic devices.

JUHA PYRHÖNEN (Senior Member, IEEE) born in Kuusankoski, Finland, in 1957. He received the Doctor of Science (D.Sc.) degree from the Lappeenranta University of Technology (LUT), Finland, in 1991.

He became a Professor of electrical machines and drives at LUT, in 1997. He is currently involved in research and development of electric motors and power-electronic-controlled drives. He has wide experience in the research and development of special electric drives for distributed power production, traction, and high-speed applications. Permanent magnet materials and applying them in machines have an important role in his research. He is also researching new carbon-based materials for electrical machines.